PyFREC 2.0: Software for Excitation Energy Transfer Modeling

Dmitri Kosenkov[1]

Correspondence to: Dmitri Kosenkov (E-mail: *dkosenkov@monmouth.edu*)

Dedicated to Ukrainian Scientists

[1] *Monmouth University, Department of Chemistry and Physics, 400 Cedar Ave., West Long Branch, NJ 07764 USA*

ABSTRACT

Excitation energy transfer is a ubiquitous process of fundamental importance for understanding natural phenomena, such as photosynthesis, as well as advancing technologies ranging from photovoltaics to development of photosensitizers and fluorescent probes used to explore molecular interactions inside living cells. The current version of *PyFREC* 2.0 is an advancement of the previously reported software (D. Kosenkov, *J. Comp. Chem.* **2016**, 37, 1847-1854). The current update is primarily focused on providing a computational tool based on Förster theory for bridging a gap between theoretically calculated molecular properties (e.g. electronic couplings, orientation factors, etc.) and experimentally measured emission and absorption spectra of molecules. The software is aimed to facilitate deeper understanding of photochemical mechanisms of fluorescence resonance energy transfer (FRET) in donor-acceptor pairs. Specific updates of the software include implementations of overlap integrals between donor emission and acceptor absorption spectra of FRET pairs, estimation of Strickler–Berg fluorescence lifetimes, calculation of Förster radii, energy transfer efficiency, and radiation zones that, in particular, determine applicability of the Förster theory.

Introduction

Our *PyFREC* software has been successfully used to model electronic couplings in complexes of organic molecules,[1] to model excitation energy transfer (EET) in the Fenna-Matthews-Olson complex,[2] phycobiliprotein,[3] and halogenated bioorthogonal boron dipyrromethene photosensitizers.[4] The current update, based on Förster theory is motivated by the need for a robust software tool which enables a better connection of computational parameters commonly obtained with molecular dynamics and electronic structure packages such as electronic couplings and orientation factors, and experimentally measured absorption and emission spectra of fluorophores, in order to understand mechanisms of energy transfer in Fluorescence Resonance Energy Transfer (FRET) pairs.[1-6] When such a comparison is done, critical questions of compatible units for spectral overlaps, adequate treatment of molar absorption (extinction) and relative intensities of emission spectra arise. Also, estimation of fluorescence lifetimes, and proper account for of fluorescence quantum yields of donors are required for meaningful interpretation of experimental and computational results. Thus, this *PyFREC 2.0* update is aimed to provide a better connection between computational and experimental data within the Förster theory formalism.

A table summarizing main features of PyFREC is provided in supporting information (S.1). In order to validate and test the software, several fluorophores and FRET pairs were considered. Fluorescence lifetimes of six common fluorophores: fluorescein, rhodamine 6G, rhodamine B, 1,4-Bis (5-phenyl-2-oxazolyl) benzene (POPOP), p-Terphenyl, and meso-derivative of 4,4-difluoro-4-bora-3a,4a-diaza-s-indacene (BODIPY) were predicted using the Strickler-Berg theory.[7] The Spectral overlap integrals and Förster radii of the fluorophores were also computed and compared with previously published computational and experimental spectroscopic data.[5,8-9] Then, BODIPY-tetrazine (TRZ) molecular probes were considered as examples of FRET systems where donor-acceptor distances and orientations affect their fluorescence intensity (Fig. 1).[10]

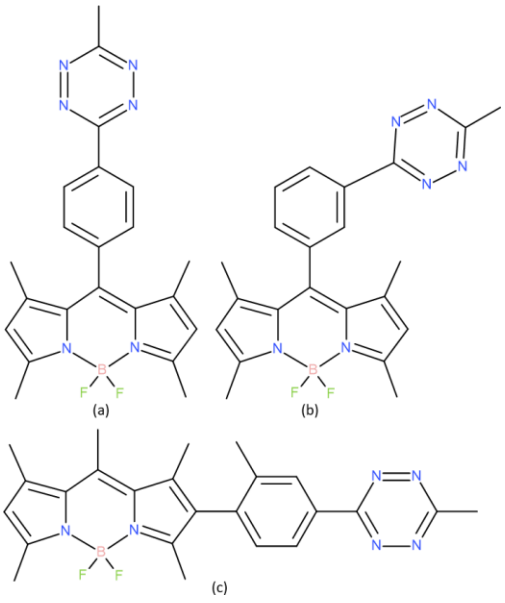

Figure 1. Excitation energy transfer in BODIPY-tetrazine (TRZ) probes (a), (b) and (c) with mutual orientations and distances between the BODIPY and TRZ moieties.

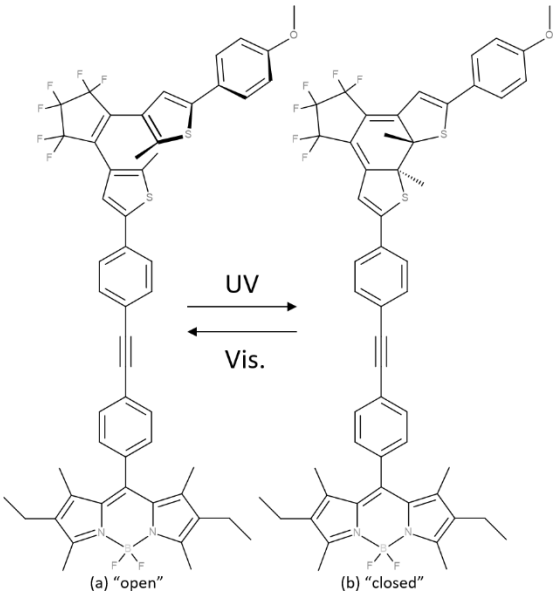

Figure 2. Excitation energy transfer in photoswitchable BODIPY- Dithienylethene (DTE) dyads in their (a) open and (b) closed forms is determined by the spectral overlap of the BODIPY and DTE moieties.

Finally, the BODIPY-dithienylethenes (DTE) molecules where the donor-acceptor spectral overlap plays a crucial role in fluorescence quenching were considered (Fig. 2).[11]

Computational Methods

One of the purposes of the *PyFREC* software is interpretation and modeling of FRET experiments that rely on EET between donor-acceptor pairs.[6] The Förster theory is commonly employed for interpretation of such results.[6,12-14] A brief summary of Förster theory implementation in *PyFREC* is given below.

Förster Energy Transfer Rates

The formulation of the Förster excitation energy transfer rate (k_{EET}) which is typically used in computational chemistry has the form:[15-16]

$$k_{EET} = \frac{2\pi}{\hbar} V^2 J_D \qquad (1)$$

where V is the electronic coupling between the donor and acceptor electronic states, and J_D is the combined density of states originating from Fermi's golden rule and commonly related to spectral overlap of donor emission and acceptor absorption spectra.[16] This expression (Eq. 1) provides a straightforward way to establish a relationship between electronic couplings and EET rates and is convenient to use if the molecular structures of the donor and acceptor are known. The electronic coupling in Eq. 1 within the Förster theory can be approximated with screened point-dipole coupling (V^0) with a linear electrostatic screening factor (*s*):

$$V = s\,V^0 \quad (2)$$

In the simplest approximation, the screening factor is defined as: $s = 1/n^2$, where n is the refractive index of the medium (solution).[17] Alternatively, exponentially attenuated transition dipole moments can be used in *PyFREC*.[2,17] The electronic coupling in Förster theory is defined as follows:

$$V^0 = \frac{\mu_D \mu_A \kappa}{{r_{DA}}^3} \quad (3)$$

where r_{DA} is the distance between centers of the donor and acceptor, μ_D and μ_A are magnitudes of transition dipole moments, and κ is the orientation factor which depends on mutual orientation of transition dipole moments (see below). Unfortunately, the factor J_D in Eq. 1 cannot be directly measured spectroscopically. In practice, if the EET rate is computed based on experimental spectra the following expression is commonly used:

$$k_{EET} = \frac{9(ln10)\kappa^2 \Phi_D J_\lambda}{\tau_D 128\pi^5 n^4 N_A r_{DA}^6} \quad (4)$$

where, Φ_D and τ_D are the fluorescence quantum yield and lifetime of the donor in the absence of the acceptor respectively. N_A is the Avogadro constant. The spectral overlap (J_λ) is defined as:

$$J_\lambda = \frac{\int_0^\infty \varepsilon_A(\lambda) F_D(\lambda) \lambda^4 d\lambda}{\int_0^\infty F_D(\lambda) d\lambda} \quad (5)$$

where $\varepsilon_A(\lambda)$ is the molar absorption of the acceptor and $F_D(\lambda)$ is fluorescence of the donor measured as functions of the wavelength λ. The spectral overlap term as defined in Eq. 3 has been recently explored in great detail.[5] It should be noted that the rate expression (Eq. 4) does not explicitly contain the electronic coupling. A detailed discussion of Eqs. 1 and 4 and related derivations were published elsewhere.[16] In the current version of *PyFREC*, Eqs. 4 and 5 are used for calculations of the Förster EET rates. The fluorescence lifetimes (τ_D) are provided by the user or computed using the Strickler-Berg equation:[7]

$$\frac{1}{\tau_D} = \frac{8000\ln(10)}{N_A} \pi n^2 c \langle {\tilde{\nu}_f}^{-3} \rangle^{-1} \frac{g_f}{g_i} \int_0^\infty \frac{\varepsilon_D(\tilde{\nu})}{\tilde{\nu}} d\tilde{\nu} \quad (6)$$

where g_i and g_f are degeneracies of the initial (excited) and final (ground) states, $\tilde{\nu}$ is the wavenumber, and $\langle {\tilde{\nu}_f}^{-3} \rangle^{-1}$ is the inverse expectation value of the ${\tilde{\nu}_f}^{-3}$ (see Eq. 7 below), and ε_D is the molar absorption of the donor. The value of $\langle {\tilde{\nu}_f}^{-3} \rangle^{-1}$ is computed based on the fluorescence spectrum:

$$\langle {\tilde{\nu}_f}^{-3} \rangle^{-1} = \frac{\int_0^\infty F_D(\tilde{\nu}) d\tilde{\nu}}{\int_0^\infty \tilde{\nu}^{-3} F_D(\tilde{\nu}) d\tilde{\nu}} \quad (7)$$

The expectation value can also be approximated as follows:[19]

$$\langle {\tilde{\nu}_f}^{-3} \rangle^{-1} = \left(\tilde{\nu}_f^{max}\right)^3 \quad (8)$$

where $\tilde{\nu}_f^{max}$ is the wavenumber at the maximum of the emission spectrum.

It is noteworthy that the Strickler-Berg fluorescence lifetime is based on the Einstein's transition probability of spontaneous emission and can be applied to modeling of strong singlet-singlet transitions but is not suitable for weak and forbidden transitions. It works best for fluorophores which have quantum yield of fluorescence values close to unity, and depends on the quality of measured absorption and emission spectra.[7]

Fragmentation Approach: Orientation Factors

PyFREC employs a fragmentation approach.[1-2] The molecular structure of the FRET pair is split into donor and acceptor molecular fragments for which transition dipole moments are computed

(usually with help of general-purpose electronic structure packages). Then, *PyFREC* aligns the molecular fragments to reconstruct the 3D molecular structure of the FRET pair.[1-2] The primary purpose of the molecular alignment is to determine a linear transformation of coordinates that brings the molecular geometry of the reference molecular fragment (donor or acceptor) to the geometry of the molecular complex (e.g., a FRET pair). In this procedure, the root-mean-square deviation between transformed (rotated and translated) coordinates of the molecular fragments ($\boldsymbol{F'}$) and corresponding coordinates of the FRET pair molecular system (***F)*** are minimized:

$$\|\boldsymbol{F'} - \boldsymbol{F}\| \longrightarrow min \quad (9)$$

After the alignment of the donor and acceptor molecular fragments to form the FRET pair, *PyFREC* automatically computes the orientation factor as follows:

$$\kappa = \tilde{\boldsymbol{\mu}}_{\boldsymbol{D}} \cdot \tilde{\boldsymbol{\mu}}_{\boldsymbol{A}} - 3(\tilde{\boldsymbol{\mu}}_{\boldsymbol{D}} \cdot \tilde{\boldsymbol{r}}_{\boldsymbol{DA}})(\tilde{\boldsymbol{\mu}}_{\boldsymbol{A}} \cdot \tilde{\boldsymbol{r}}_{\boldsymbol{DA}}) \quad (10)$$

where $\tilde{\boldsymbol{\mu}}_{\boldsymbol{D}}$ and $\tilde{\boldsymbol{\mu}}_{\boldsymbol{A}}$ are normalized transition dipole moments of the donor and acceptor fragments respectively, and $\tilde{\boldsymbol{r}}_{\boldsymbol{DA}}$ is the normalized vector connecting the donor and acceptor. As the EET rate is proportional to κ^2 (Eq. 4) the squared value of the orientation factor is commonly used. This factor is in the range: $0 \leq \kappa^2 \leq 4$, which follows from its definition. The commonly used averaged value is $\kappa^2 = 2/3$, which corresponds to random isotropic rotation of the donor and acceptor.[20] Although *PyFREC* automatically computes the orientation factor for provided molecular geometries of FRET pairs, the (averaged) value of the orientation factor can be directly specified by the user.

Additional Characteristics of Excitation Energy Transfer

Additionally, *PyFREC* computes the efficiency of the EET of a single donor-acceptor pair as :[6]

$$E = \frac{k_{EET}}{k_{EET}+1/\tau_D} \quad (11)$$

One should note that the efficiency (E) defines the rate of Förster EET relative to the total rate ($k_{EET} + 1/\tau_D$), which accounts for the Förster EET rate of fluorescence. Thus, EET efficiency can be significant (e.g. $E \geq 50\%$) if $k_{EET} \geq 1/\tau_D$ even if the orientation factor is small: $\kappa \ll 50\%$.[21] *PyFREC* also computes the Förster radii of fluorophores:

$$R_o^6 = k_{EET}\tau_D r_{DA}^6 \quad (12)$$

The Förster radius corresponds to the donor-acceptor distance at which $k_{EET} = 1/\tau_D$ and the EET efficiency is 50%.[6] Then the EET rate can be alternatively expressed as: $k_{EET} = R_o^6/\tau_D r_{DA}^6$.

It also important to consider that Förster theory is applicable when the donor-acceptor distance belongs to the near field zone. In the theory of radiation, radiative regions (zones) are defined based on distance (b):[6]

$$b = \frac{\lambda}{2\pi n} \quad (13)$$

where λ is the wavelength of radiation. The value of distance b is used to distinguish radiation zones: Dexter ($0 < r_{DA} < 0.01b$), near-field ($0.01 < r_{DA} < 0.1b$), intermediate ($0.1b < r_{DA} < 10b$), and far field or radiation zone ($10b < r_{DA}$). Förster theory is valid in the near-field zone which is typically in the range of 1-10 nm. *PyFREC* automatically computes the distance b and reports to which radiation zone r_{DA} belongs to.

Software Architecture and Implementation

A general view of the PyFREC structure is shown in Scheme 1. The software consists of several modules that provide reading and initial processing of input data: configuration manager, calculation manager, excited states reader, reader of molecular structures, and a module that performs alignment of molecular

fragments. Once the information on excited states and molecular structures is received, *PyFREC* identifies potential resonances between electronic excited states of fragments, calculates spectral overlaps, and computes electronic couplings.

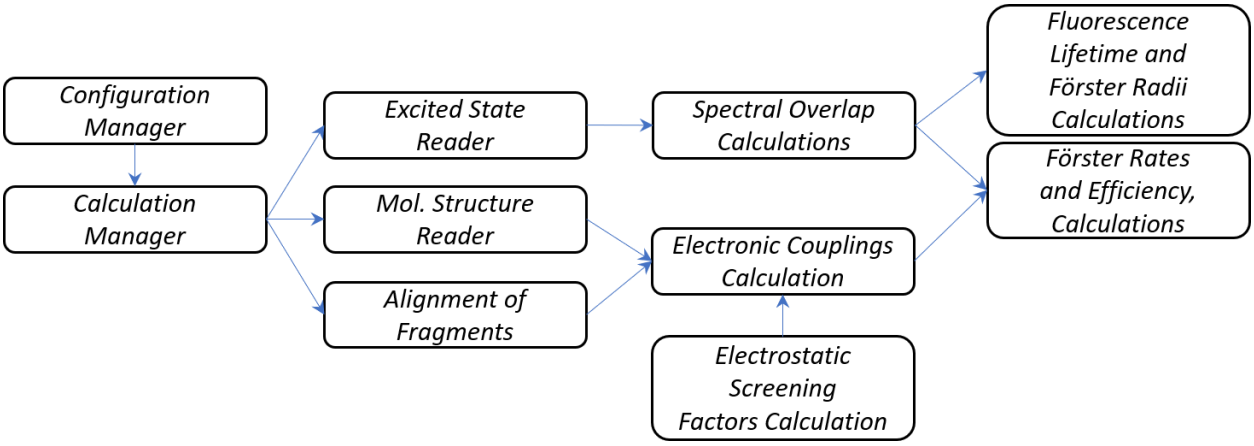

Scheme 1. *PyFREC* software structure (see details in text).

The coupling calculation module calls the module that computes electrostatic screening factors. Rates of excitation energy transfer are further computed using Förster theory. There also are shared auxiliary library modules that store constants, conversion factors, standard data structures (e.g., atoms, Cartesian coordinates, etc.) and routines for data exchange among other modules. While many common standard Python libraries are used by *PyFREC* (e.g., *os, sys, re*, etc.),[22] the computationally intensive routines (matrix algebra, integration of differential equations, etc.) rely on *NumPy* and *SciPy* libraries.[23-24] A list of required packages is provided in supporting information (S.2). *PyFREC* is a command line tool (all input and output files are in text format). The user provides definitions of molecular fragments and parameters of the simulation. The main user input file contains the following sections: *"Methods"*, *"Molecular System"* and definitions of molecular fragments. The section *"Methods"* defines the type of calculations to be requested (e.g., calculation of electronic couplings). The *"Molecular System"* section defines general parameters of the entire system (e.g., a PDB file with the molecular structure of the FRET pair). In addition, properties of each molecular fragment (e.g., excitation energies and transition dipole moments) are provided in a separate input file for each fragment. These properties of the fragment are usually computed with general-purpose electronic structure packages. *PyFREC* is open-source software. The source code along with user manual, sample input and output files are available free of charge at https://github.com/DKosenkov/PyFREC

Results and Discussion

In order to illustrate functionality of the *PyFREC* software and validate computational methods used, results of calculations with the described modules of *PyFREC* are presented below. All inputs and outputs for each of the presented calculations are provided along with the *PyFREC* distribution. Computational details for electronic structure calculations on molecular fragments (e.g., geometry optimization, transition dipole moments calculations) are provided in

supporting information (S.4). Absorption and emission spectra of fluorophores are obtained from *PhotochemCAD* [8,9] except for spectra of BODIPY-DTE dyads[11] (see also supporting information S.5 for the spectral input preparation procedure) and tetrazine.[29]

Fluorescence Lifetimes

The fluorescence lifetime is a required parameter for calculation of EET rates in the Förster theory. In *PyFREC,* the fluorescence lifetime is estimated using the Strickler-Berg approach (Eq. 6).

Alternatively, fluorescence lifetime may be provided as part of the user input. Sample calculations of the fluorescence lifetimes of some common chromophores are presented in Table I.

Computation of lifetimes requires knowledge of the molar extinction of the chromophore. There are two alternative equations for calculation of the inverse expectation value of $\tilde{\nu}_f^{-3}$: numerical integration of the emission spectrum (Eq. 7) o a simplified equation (Eq. 8) that uses only the position of the emission maximum. These two approaches produce slightly different lifetimes, listed in Table I as $\tau_{calc\text{-}1}$ and $\tau_{calc\text{-}2}$, calculated with the simplified and full numerical integration respectively. The refractive index of the solution and the quantum yield of the chromophore are used as input parameters for the calculation.

Computed fluorescence lifetimes of fluorescein, Rhodamine B, and BODIPY are within 10% of the experimental values. Lifetimes for Rhodamine 6G, POPOP, and p-Terphenyl are predicted within the 20%. One may note that absorption spectra are commonly reported in their normalized forms (maximal absorbance set to 1). However, the absorption spectra (see Eq. 6) are multiplied by the molar extinction coefficient, which is in the range of 10^4-10^5 $M^{-1}cm^{-1}$, for the considered molecules. Thus, the method is sensitive to the quality of the absorption spectra.

The approximated method for calculation of the inverse expectation value of ($\tilde{\nu}_f^{-3}$) of the fluorescence spectrum: $\tau_{calc\text{-}1}$ based on the Eq. 2.8 gives an averaged unsigned percent error of 10%. The averaged unsigned percent error for the method based on the complete numerical integration of the emission spectrum (Eq. 7): $\tau_{calc\text{-}2}$ produces comparable values of 11%, probably due to its higher sensitivity to the line shape of the emission spectrum which, in particular, is dependent on vibrionic structure not accounted for in the Strickler-Berg theory. Overall, based on data in Table I, the averaged error in prediction of the fluorescence lifetimes with either method is close to 10% (maximum error is 20%).

Additionally, in order to validate calculations of spectral overlaps, the homotransfer properties of chromophores were computed: overlap of the emission and absorption spectra (Eq. 3) for the same chromophore. Computed spectral overlap values for fluorescein (J= $1.29x10^{14}$ M^{-1} $cm^{-1}nm^4$) and rhodamine 6G (J = 1.96 $x10^{15}$ M^{-1} $cm^{-1}nm^4$) exactly reproduce the values published previously.[5] Forster Radii of the chromophores were also computed (R_F). The predicted value for BODIPY is 4.3 nm which is slightly shorter than 4.5-4.8 nm based on experimental determination.[11] The distance parameter b is in the range of 61-63 nm for all considered fluorophores. This defines donor-acceptor distances where the Förster theory is valid from the radiation theory standpoint (near field zone) as 0.61-6.3 nm.

EET in BODIPY- Dithienylethene (DTE)

The BODIPY-DTE dyad is a photoswitchable molecule (Fig. 3) which undergoes reversible isomerization from an open fluorescent form to a closed non-fluorescent form under irradiation with UV light (Fig. 2),[11] forming a photostabilized mixture.

Table I. Fluorescence lifetimes measured experimentally (τ_{exp}) and calculated using the Strickler-Berg theory with approximated (τ_{calc-1}) or full numerical integration of emission spectra (percent errors are given in parentheses). Properties of fluorophore solutions used for calculations: refractive index of the solution (n), molar absorption coefficient (ε), absorption (λ_{abs}) and emission (λ_{ems}) spectra and fluorescence quantum yield (Φ_D); computed excitation energy homotransfer properties: spectral overlaps (J) and Förster radii (R_F, nm). Distance parameter (b, nm) defines the distance range: b/100 - b/10 where the Förster theory is valid.

Chromophore	Solvent	n	ε, $M^{-1}cm^{-1}$	λ_{abs}, nm	λ_{ems}, nm	Φ_D	τ_{exp}, ns	τ_{calc-1}, ns	τ_{calc-2}, ns	J, $M^{-1}\,cm^{-1}nm^4$	R_F,[i] nm	b, nm
Fluorescein[a]	Ethanol[f]	1.3611	9.23×10^4	500	540	0.97	4.25[c]	3.98 (-6%)	4.37 (3%)	1.29×10^{14} [j]	3.6	63.1
Rhodamine 6G[a]	Ethanol	1.3611	1.16×10^5	530	552	0.95	3.99[c]	3.27 (-18%)	3.62 (-9%)	1.96×10^{15} [j]	5.6	64.6
Rhodamine B[a]	Ethanol	1.3611	1.06×10^5	543	565	0.70	2.69[d]	2.66 (-1%)	2.88 (7%)	2.36×10^{15}	5.5	66.1
POPOP[a,b]	Cyclohexane	1.4235	4.70×10^4	359	408	0.93	1.12[e]	1.27 (13%)	1.34 (20%)	7.96×10^{13}	3.2	45.6
p-Terphenyl[a]	Cyclohexane	1.4235	3.38×10^4	276	338	0.93	0.98[e]	1.10 (12%)	1.18 (20%)	2.27×10^{12}	1.8	37.7
BODIPY[g]	Dichloromethane	1.4240	5.60×10^4 [h]	527	547	0.60	4.3[g]	3.85 (-10%)	4.46 (4%)	6.85×10^{14}	4.3[k]	61.1

[a] Experimental absorption and emission spectra are obtained from Ref. 9. [b] 1,4-Bis(5-phenyl-2-oxazolyl)benzene; [c] Ref. 25; [d] Ref. 26; [e] Ref. 27; [f] Basic solution; [g] *Meso*-derivative of boron-dipyrromethene Ref. 11; [h] Molar absorption of the BODIPY *meso*-substitute derivates Ref. 28; [i] Based on the lifetime τ_{calc-2}; [j] The value exactly reproduces overlaps Ref. 5 for software validation. [k] The experimental value of the Förster radius is 4.5-4.8 nm according to Ref. 11.

Table II. Förster-type energy transfer in the BODIPY-DTE dyad: DTE molar absorption (ε) maximum λ_{abs}; BODIPY emission maximum λ_{ems}; Predicted with TD-DFT excited state S_1 (E_{S1}); Energy gap (ΔE) between lowest singlet states (S_1) of BODIPY and DTE; Magnitude of the transition dipole moment of DTE (μ_{DTE}); BODIPY-DTE distance (R), Squared donor-acceptor orientation factor (κ^2) and its relative value (%); Electronic couplings without (V) and with the electrostatic screening (cV); Spectral overlap (J), and Energy transfer rate k, and efficiency (E)

Isomer/Form	λ_{abs},[a] nm	λ_{ems},[a] nm	ε,[a, b] $M^{-1}cm^{-1}$.	E_{S1}, nm	ΔE, cm^{-1}	μ_{DTE}, Debye	R, nm	κ^2	V,[c] cm^{-1}	cV,[d] cm^{-1}	J, $M^{-1}\,cm^{-1}nm^4$	k, s^{-1}	E[e], %
Closed/ non-fluorescent	354,608	-	3.56×10^4	541	3182	8.87	1.6	4.60×10^{-3} (0.1%)	6.4	3.2	1.09×10^{15}	8.86×10^8	79
Open/ Fluorescent	328	547	4.05×10^4	462	10051	11.66	1.6	3.38×10^{-2} (0.8%)	22.3	11.0	0	0	0

[a] Experimental absorption and emission spectra are obtained from Ref. 11. [b] Relative absorption maxima of DTE measured with respect to the BODIPY absorption maximum (see S2.1 for details); [c] Coupling is based on the computed transition dipole moment of BODIPY: 8.67 D.; [d] Electrostatic screening factor for the dichloromethane is $c = 1/n^2 = 0.493$; [e] Efficiency is based on the fluorescence lifetime of the BODIPY donor: 4.3 ns Ref. 11.

Weak fluorescence in the photostabilized mixture (mainly from the non-fluorescent closed form) was registered and was attributed to the 4% of the open form being present.[11] It was suggested that Förster-like energy transfer from the donor BODIPY moiety to the DTE (dithienylethene) acceptor takes place in the closed form which quenches its fluorescence.

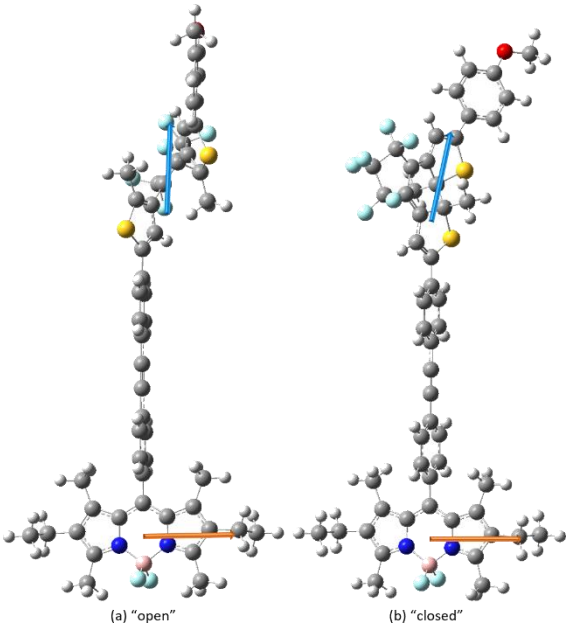

Figure 3. Photoswitchabe BODIPY - Dithienylethene (DTE) dyads (a) open and (b) closed forms; arrows show directions of normalized transition dipole moments (TDM) of BODIPY (gold) and DTE (teal). Excitation energy transfer is primarily determined by the spectral overlap.

Published steady state emission and absorption spectra of BODIPY-DTE dyads[11] were analyzed and taken as input for *PyFREC* 2.0. Additionally, molecular structures of the open and closed forms of the BODIPY-DTE dyads were computed with DFT. Transition dipole moments of BODIPY and DTE moieties were computed with the TD-DFT (details provided in supporting information S.5-S.6). Then, the obtained data were used as input for *PyFREC*. The main input parameters and obtained results are presented in Table II. The experimental data suggest that, in addition to the absorption maximum at 354 nm, the closed form of DTE has a peak around 608 nm which is close to the emission maximum of BODIPY at 547 nm. On the contrary, the open form has an absorption maximum of DTE only at 328 nm which is unlikely to overlap with the BODIPY emission at 547 nm.

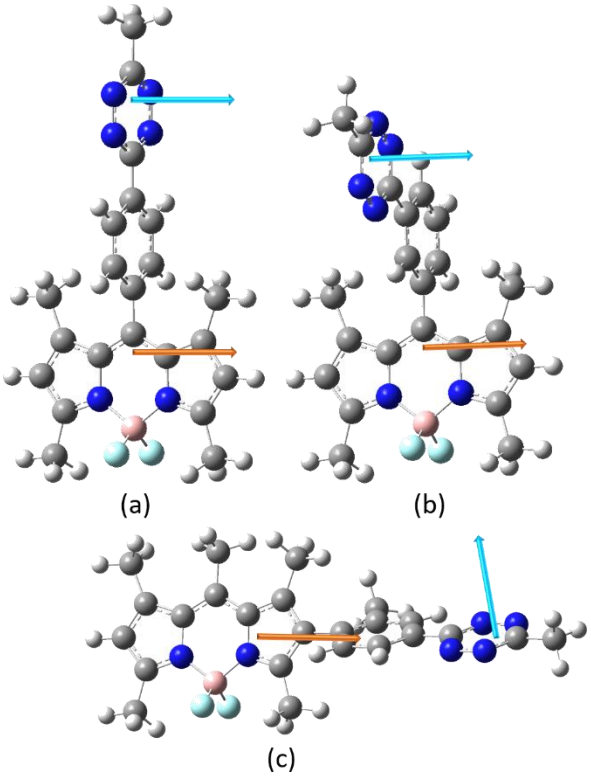

Figure 4. BODIPY-tetrazine (TRZ) probes (a), (b), and (c); arrows show directions of normalized transition dipole moments (TDM) of BODIPY (gold) and TRZ (teal). Excitation energy transfer rates are primarily determined by the orientation factors and donor-acceptor distances.

The calculated overlap integral between the BODIPY emission and DTE absorption in experimental spectra is $J=1.09\times10^{15}$ M^{-1} $cm^{-1}nm^4$ in the closed form and J=0 in the open form. The TD-DFT results are also in line with this finding: The DTE acceptor has absorption at 541 nm and 462 nm in the closed and open forms

respectively. According to the TD-DFT, the S1 excited state of BODIPY is 3182 cm^{-1} shifted off-resonance from the S_1 state of DTE in the closed form and almost triple that value: 10051 cm^{-1} in the open form. This makes the BODIPY-DTE resonance excitation energy transfer unlikely in the open form.

Interestingly, while the donor-acceptor distances in open and closed forms are nearly the same (1.6 nm), the transition dipole moment of DTE increases upon opening from 8.87D to 11.66D. It is noteworthy that orientation factors while still under 1% also increase upon opening. As a result, the electronic coupling increases from 3.2 cm^{-1} to 11.0 cm^{-1} upon opening. However, structural data from TD-DFT simulations suggest only $\kappa^2=4.6\times10^{-3}$ (0.1%) as the value of the squared orientation factor and Förster electronic coupling of 3.2 cm^{-1} (which accounts for the electrostatic screening due to dichloromethane solvent). The corresponding EET rate is 8.86×10^{8} s^{-1} with the 79% EET efficiency. The experimental spectroscopic findings suggest the $6.7\text{-}10\times10^{10}$ s^{-1} EET rate which is probably due to contributions from non-Förster mechanisms (e.g. through-bond energy transfer or TBET, vibrationally-assisted energy transfer, etc.[11-30]).

In summary, the results based on experimental steady state absorption and emission spectra and computed TD-DFT results indicate that the open form is fluorescent (no EET present) due to the absence of spectral overlap between the BODIPY and DTE regardless of their mutual orientation and electronic coupling. In the closed form, while qualitatively correct, the predicted EET rate is significantly underestimated probably due to non-Förster energy transfer mechanisms.

BODIPY-Tetrazine (TRZ)

Three types of BODIPY-Tetrazine (TRZ) probes where BODIPY acts as a donor and TRZ as an acceptor (Fig. 4) have been considered. These probes show substantial increases in fluorescence as a result of their reactions with trans-cyclooctenol TCO that effectively eliminates the TRZ acceptor.[10] It has been suggested that fluorescence quenching in the BODIPY-TRZ probes is due to excitation energy transfer either via FRET or TBET mechanisms.[10,30]

Table III. Förster-type energy transfer in BODIPY[a]-Tetrazine(TRZ)[b] probes: fluorescence intensity increase of BODIPY upon reaction of the tetrazine (I_{fl}) and corresponding relative values ($I_{fl\text{-}rel}$); BODIPY-TRZ distance (R), Squared orientation factor (κ^2) and its relative value (%); Electronic couplings without (V) and with the electrostatic screening (cV); Energy transfer rate (k), its relative value (k_{rel}) and efficiency (E)

Probe	I_{fl}[a]	$I_{fl\text{-}rel}$[a]	R, nm	κ^2	V,[c] cm^{-1}	cV,[d] cm^{-1}	k, s^{-1}, [e]	k_{rel}	E, %
(a)	340	0.31	0.8	1.00 (25%)	65.2	36.1	4.03×10^{11}	0.63	99.94
(b)	1100	1.00	0.7	1.00 (25%)	99.6	55.1	9.38×10^{11}	1.00	99.98
(c)	120	0.11	0.9	2.61×10^{-3} (0.1%)	2.4	1.3	4.62×10^{8}	0.00	66.51

[a] Spectral properties of BODIPY are obtained from Ref. 11. [b] Spectral properties of TRZ used in simulations are: molar extinction (615 $M^{-1}cm^{-1}$), absorption maximum (562 nm) are obtained from Ref. 29; [c] The following calculated transition dipole moments of BODIPY were used: probes (a) and (b): 7.8 D; (c): 8.6 D; and TRZ: 0.89 D. [d] Electrostatic screening factor for the acetonitirille is $c = 1/n^2 = 0.554$; [e] The spectral overlap is $J=3.06\times10^{13}$ M^{-1} cm^{-1} nm^4

Upon elimination of TRZ acceptors the BODIPY fluorescence intensity is substantially increased in all probes (I_{fl}, Table III). Based on these values, the relative increase in fluorescence intensities ($I_{fl\text{-}rel}$) were further used as a measure of the fluorescence quenching efficiency in BODIPY-

TRZ probes. Thus, the greater value of $I_{fl\text{-}rel}$ corresponds to more efficient (fast) EET in the BODIPY-TRZ dyad. The TD-DFT method was used to determine mutual positions and orientations of BODIPY and TRZ moieties and transition dipole moments (see supporting information S.7 for details). Photochemical parameters for the BODIPY moiety were used the same as for BODIPY-derivative in BODIPY-DTE Dyad due to their similarity and availability of data. Parameters used for FRET simulations in *PyFREC* are listed in Table III.

The BODIPY-TRZ distances in probes increase: 0.7, 0.8, and 0.9 in probes b, a, and c respectively. Probes a and b have substantially large orientation factors (25%) and probe c has an orientation factor close to zero (0.1%). Probe c has been specifically designed to have zero orientation factor to minimize the FRET energy transfer.[11] The screened electronic couplings are: 55.1 cm^{-1} and 36.1 cm^{-1} for probes b and c due to their relatively short BODIPY-TRZ distances and large orientation factors. It should be noted that all three probes are assumed to have the same BODIPY-TRZ spectral overlap computed with the experimental emission of BODIPY[11] and absorption of TRZ[29] spectra. The FRET rate constant suggests fastest EET in probe b followed by probe a. Probe c has the slowest EET rate due to minimal orientation and maximal donor-acceptor distance.

The relative efficiency of the FRET has demonstrated that all three probes have >50% EET efficiency due to relatively fast EET rates as compared to the BODIPY fluorescence rate: $k_D = 1/\tau_D \quad = 1/4.3\,ns \quad = 2.33 \times 10^8\,s^{-1}$. Efficiency of energy transfer as defined in Eq 2.11 depends upon the relative rate of EET as compared to the rate of fluorescence (inverted fluorescence lifetime). Therefore, even with low orientation factors (e.g. BODIPY-TRZ, (c) ~0.1%), if the Förster rate ($k=4.62\times10^8\ s^{-1}$) is close to the fluorescence rate ($2.33 \times 10^8\,s^{-1}$) the EET efficiency may be significant: 66.3%. It can be generalized, that fluorescence of FRET donors with longer fluorescence lifetimes can be more efficiently quenched by EET even at perpendicular orientations of donor and acceptor moieties and relatively low orientation factors. Finally, the trend in increasing relative EET rates (k_{rel}) matches the observed trend in relative fluorescence increase ($I_{fl\text{-}rel}$). The fluorescence increase (I_{fl}) is defined as: $I_{fl}=I/I_q$, where I is the intensity of BODIPY fluorescence without a quencher (assumed to be nearly the same in all considered probes), and I_q is the intensity of the fluorescence in the presence of a TRZ quencher. Therefore, BODIPY fluorescence increases more when there is a higher EET rate to TRZ in the quenched state of the probe (i.e. smaller value of I_q). This suggests that the BODIPY fluorescence is quenched as a result of energy transfer to TRZ.

Conclusions

The updated version of *PyFREC* software presented here is designed to provide a robust tool for Förster theory simulations. The software implements calculation of Strickler–Berg fluorescence lifetimes, electronic couplings, orientation factors, spectral overlaps, Förster radii, excitation energy transfer rates and efficiencies. Sample applications of the software are provided to predict fluorescence lifetimes of some common chromophores that resulted in average 10% (and maximal 20%) differences from experimentally determined values. The energy transfer and fluorescent quenching mechanisms have been investigated in BODIPY-DTE and BODIPY-TRZ systems. In BODIPY-DTE, the primary mechanism for fluorescence quenching upon the photoisomerization (ring opening) is attributed to the dramatic decrease in spectral overlap between the BODIPY donor and DTE acceptor moieties. In the BODIPY-TRZ probes, relative fluorescence quenching was attributed to a combination of mutual donor-acceptor orientation factors (decreased from 25 to 0%) and donor-acceptor distances (increased

from 0.7 to 0.9 nm). Relative energy transfer rates and fluorescence quenching predictions in BODIPY-DTE and BODIPY-TRZ are satisfactorily close to experimental observation. Nevertheless, it can also be concluded that even at low orientation factors (~0.1%) the Förster rates still may be comparable [e.g., in BODIPY-TRZ (c)] to the rates of fluorescence and quench the donor's fluorescence. The computed absolute Förster rates are underestimated as compared with rates observed experimentally. This suggests the need for consideration of other energy transfer mechanisms, including vibrationally assisted and/or through-bond energy transfer mechanisms, as was suggested by previous studies.[10-11] Thus, future developments of *PyFREC* are needed to include energy transfer mechanisms beyond the Förster theory. In future releases of the PyFREC software we are planning to add quantum master equation, vibrationally-assisted, exchange (e.g. Dexter), and singlet-triplet energy transfer modeling methods.

Funding Information

The project was funded in part by the National Science Foundation CHE-1955649 RUI-D3SC and the Donors of the American Chemical Society Petroleum Research Fund for partial support of this research though grant #58019-UR6.

Keywords: Förster, FRET, Exciton, BODIPY, Bioorthogonal Chemistry

Supporting Information

Additional Supporting Information may be found in the online version of this article.

Data Availability Statement

The data that support the findings of this study are openly available in GitHub at https://github.com/DKosenkov/PyFREC

References and Notes

1. D. Kosenkov, *J. Comp. Chem.* **2016**, 37, 1847-1854.
2. Y. Kholod, M. DeFilippo, B. Reed, D. Valdez, G. Gillan, and D. Kosenkov, *J. Comp. Chem.* **2018**, 39, 438-449.
3. Y. K. Kosenkov and D. Kosenkov, *J. Chem. Phys.* **2019**, 151, 144101.
4. G. Linden, L. Zhang, F. Pieck, U. Linne, D. Kosenkov, R. Tonner, and O. Vazquez, *Angew. Chem. Int. Ed.* **2019**, 58, 12868-12873.
5. Q. Qi, M. Taniguchi, J. S. Lindsey *J. Chem. Inf. Model.* **2019**, 59, 652−667.
6. B. W van der Meer, In FRET−Förster Resonance Energy Transfer (FRET)−From Theory to Applications; I. Medintz, N. Hildebrandt, Eds.; Wiley VCH: Weinheim, **2014**; Chapter 3, pp 23−62.
7. S. J. Strickler, R. A. Berg, *J. Chem. Phys.* **1962**, 37, 814-822.
8. M. Taniguchi, H. Du, J. S. Lindsey. *Photochem. Photobiol.* **2018**, 94, 277–289.
9. M. Taniguchi, J. S. Lindsey, *Photochem. Photobiol.* **2018**, 94, 290–327.
10. J. C. T. Carlson, L. G. Meimetis, S. A. Hilderbrand, R. Weissleder, *Angew. Chem. Int. Ed.* **2013**, 52, 6917-6920.
11. F. Schweighöfer, L. Dworak, C. A. Hammer, H. Gustmann, M. Zastrow, K. Rück-Braun, J. Wachtveitl. Highly efficient modulation of FRET in an orthogonally arranged BODIPY–DTE dyad. *Sci. Rep.* **2016,** 6, 28638.
12. T. Förster, *Naturwissenschaften*, **1946**, 33, 166–175.
13. T. Förster, *Faraday Discuss.*, **1959**, 27, 7–17.
14. Th. Förster, *Delocalized Excitation and Excitation Transfer*; Florida State University: Tallahassee, Fl. **1965**.
15. C. Curutchet, B. Mennucci, *Chem. Rev.* **2017**, 117, 294-343.

16. V. May, O. Kühn, *Charge and Energy Transfer Dynamics in Molecular Systems*, 3rd Ed. Wiley VCH: Weinheim, **2011.**
17. T. Renger, *Photosynth Res*, **2009**, 102, 471-485.
18. C. Curutchet, G. D. Scholes, B. Mennucci, R. Cammi, *J. Phys. Chem. B*, **2007**, 111, 13253-13265.
19. B. Cohen, C. E. Crespo-Hernandez, B. Kohler, *Faraday Discuss.* **2004**, 127, 137–147.
20. B. W. van der Meer, D. M. van der Meer, S. S. Vogel, In FRET−Förster Resonance Energy Transfer (FRET)−From Theory to Applications; I. Medintz, N. Hildebrandt, Eds.; Wiley VCH: Weinheim, **2014**; Chapter 4, pp. 63-104.
21. J. S. Lindsey, M. Taniguchi, D. F. Bocian, D. Holten, **2021**, *Chem. Phys. Rev.* 2, 011302.
22. The Python Standard Library https://docs.python.org/2.7/library/ (Accessed Mar 2, 2022)
23. NumPy https://numpy.org/ (Accessed Mar 2, 2022)
24. SciPy https://www.scipy.org/ (Accessed Mar 2, 2022)
25. D. Magde, R. Wong, P. G. Seybold, *Photochem. Photobiol.* **2002**, 75, 327-334.
26. A. S. Kristoffersen, S. R. Erga, B. Hamre, Ø. Frette*, J. Fluoresc.* **2014**, 24, 1015–1024.
27. N. Boens, W. Qin, N. Basarić, J. Hofkens, M. Ameloot, J. Pouget, J.-P. Lefèvre, B. Valeur, E. Gratton, M. vandeVen, N. D. Silva, Y. Engelborghs, K. Willaert, A. Sillen, G. Rumbles, D. Phillips, A. J. W. G. Visser, A. van Hoek, J. R. Lakowicz, H. Malak, I. Gryczynski, A. G. Szabo, D. T. Krajcarski, N. Tamai, A. Miura. *Anal. Chem.* **2007**, 79, 2137–2149.
28. Y. Kubota. In: Progress in the Science of Functional Dyes; Y. Ooyama, S. Yagi, Eds.; Springer: Singapore, **2021;** pp. 119-220.
29. R. M. Hochstrasser, D. S. King, A. B. Smith III, *J. Am. Chem. Soc.* **1977**, 99, 3923–3933.
30. D. Cao, L. Zhu, Z. Liu, W. Lin. *J. Photochem. Photobiol. C: Photochem. Rev.* **2020**, 44, 100371.

GRAPHICAL ABSTRACT

Dmitri Kosenkov

PYFREC 2.0: SOFTWARE FOR EXCITATION ENERGY TRANSFER MODELING

PyFREC 2.0 is the excitation energy transfer modeling software. The main goal of this tool is to integrate electronic structure computed and experimentally measured spectroscopic data. The input information on molecular structure, transition dipole moments, and steady-state absorption and emission spectra is used to predict fluorescence lifetimes with the Strickler–Berg fluorescence lifetimes, Förster radii, orientation factors, and energy transfer rates and efficiencies.

GRAPHICAL ABSTRACT FIGURE